Journal of Membrane Science 475 (2015) 320–329

Contents lists available at ScienceDirect

Journal of Membrane Science

journal homepage: www.elsevier.com/locate/memsci

Experimental characterization and numerical simulation of the anti-biofuling activity of nanosilver-modified feed spacers in membrane filtration

Avner Ronen, Sofia Lerman, Guy Z. Ramon, Carlos G. Dosoretz *

Faculty of Civil and Environmental Engineering and Grand Water Research Institute, Technion-Israel Institute of Technology, Haifa 32000, Israel

ARTICLE INFO

Article history:
Received 11 May 2014
Received in revised form
17 October 2014
Accepted 18 October 2014
Available online 28 October 2014

Keywords:
Feed spacer
Biofouling
Nanosilver
Membrane separation
Numerical simulation

ABSTRACT

The antibiofouling activity of nanosilver-coated feed spacers was investigated in a crossflow membrane filtration-cell system simulating the conditions in spiral wound modules. Silver ions distribution in the feed channel and near the membrane was estimated by numerical simulation. Nanosilver was embedded into the polypropylene network using sonochemical deposition. The ability of the modified spacer to hinder biofilm development on the adjacent membranes was studied at 0.15 ms^{-1} crossflow velocity, using polysulfone ultrafiltration membrane exposed to a mixed microbial enrichment. The physical properties of the modified spacer and biofilm development were evaluated using scanning electron microscopy and confocal laser scanning microscopy imaging (HRSEM and CLSM). HRSEM images depicted significantly less bacteria attached to the membranes near the modified spacer, mainly scattered with a sporadic monolayer structure. Dead/live staining assay by CLSM indicated a significantly higher percentage of dead bacteria cells attached to the membranes adjacent to the modified spacer in comparison to untreated spacers (control). The silver modified spacers displayed improved and steadier permeate flux along the 10 days of the run compared to the control. Flow and mass transfer simulations showed increased silver ions concentration near the membrane as a function of the spacer configuration. The life span of the modified spacer was evaluated as well.

1. Introduction

Pressure driven membrane filtration processes, i.e. reverse osmosis (RO) and nanofiltration (NF) can produce high quality drinking water from a variety of impaired sources including brackish water [1]. The 'Achilles heel' of all membrane processes is bacterial adhesion to the membrane surface and the ensuing biofilm formation [2]. Many species of bacteria form biofilms, which are extremely difficult to remove [3,4]. Biofilm development was found to be exacerbated by the permeation through the membrane, where the transport of organic matter, nutrients and bacteria toward the membrane causes the buildup of a biofouling layer [5], eventually resulting in a decrease of permeate flux and increased energy demands. The most dramatic effect on membrane permeability decline is thought to be due to the formation and accumulation of exopolymeric substances (EPS) [6,7].

The most common commercial RO configuration is the spiral wound module, which offers a high membrane surface area to volume ratio. This configuration includes polymeric separation grids (i.e. spacers) which separate the membrane sheets, maintaining an open flow path while also providing flow disturbances that may contribute to reduced concentration polarization. However, it has also been observed that the spacers also create regions of recirculation and low velocities (i.e., stagnation points) that tend to increase the propensity for biofouling. Biofilm formation on the spacer has been identified as the source of membrane biofouling and, hence, has attracted interest in recent years, studied both experimentally [8–11] and via numerical simulations [12–14].

As a strategy for minimizing fouling, several attempts have been reported where the spacer has been modified. For example, commercial "low fouling" elements are fabricated with polymeric biostatic feed spacers containing 0.5 wt% triclosan [15], an effective antibacterial agent. Data provided by the manufacturer show reduced biofouling tendency and pressure drop over a month in a lab-scale system and in a commercial size RO module. Another approach for spacer modification reported by Hausman et al. [16] includes creating antibacterial polypropylene films through surface functionalization by a 'spacer arm' with metal chelating ligands charged with copper ions. Results reported in the literature are inconclusive regarding the efficiency to eliminate biofouling through spacer modification. Yang et al. [9] showed that by coating the spacer and membrane with nanosilver they could maintain a higher permeate flux and rejection for 20 days in an RO membrane

* Corresponding author. Tel.: +972 4 8294962; fax: +972 4 8228898.
E-mail address: carlosd@tx.technion.ac.il (C.G. Dosoretz).

http://dx.doi.org/10.1016/j.memsci.2014.10.042
0376-7388/

system. In addition, Araújo et al. [10] showed a decrease in the feed channel pressure drop and biomass concentration after 15 days of operation by using different antibacterial spacer coatings (i.e. copper, silver and gold) although biofilm formation could not be completely prevented. In contrast, Miller et al. [17] coated the membrane and spacer by polydopamine and poly[ethylene glycol] with no significant influence on pressure drop in the feed channel and biomass found on the membrane and spacers. Recently, Ronen et al. [18,19] showed that biofouling could be efficiently restricted by modification of commercial polypropylene feed spacers applying nano-zinc sonochemical deposition.

Silver compounds and silver ions have been long known to possess bactericidal effects as well as a broad spectrum of antimicrobial activities [20,21]. Silver nanoparticles show enhanced ability due to their increased active surface area – particles of less than 10 nm were found to be more toxic to bacteria and could even inhibit certain viruses [22]. Despite the vast number of papers regarding the antimicrobial effects of nanolsilver [23–25], the mechanisms by which silver nanomaterials exert their antimicrobial activity are only partly agreed upon. It was found that at low concentrations (micromolar) silver ions interact with enzymes of the respiratory chain reaction such as NADH dehydrogenase, resulting in the uncoupling of respiration from ATP synthesis. The interaction with respiratory and transport proteins is due to the high affinity of silver ions with thiol groups present in the cysteine residues of those proteins [26,27]. Furthermore, while reactive oxygen species (ROS) are natural byproducts of the metabolism of respiring organisms, their presence can be controlled by antioxidant enzymes. Silver ions can hinder these enzymes through direct interactions with thiol groups in the superoxide radical scavenging enzymes. Therefore, inducing ROS generation which damages the cells [28].

Coating and/or embedment of nanosilver in a carrying polymeric matrix has been reported, achieved through both mechanical and chemical methods including electro-spinning, polymer blending and sonochemical deposition [29–31]. Sonochemical deposition has shown promising abilities for coating or embedding nanosilver into several materials including polymers, glass, wool and even metals [31–36].

In the present study, the concept of an antibacterial feed spacer containing nanosilver was evaluated for its ability to suppress biofilm development during membrane filtration. Spacer modification was achieved via sonochemistry, which enabled the deposition of silver nanoparticles onto the surface of the feed spacer with minimal impact on its geometry and, hence, its hydrodynamic influence. Biofilm development using modified spacers was monitored experimentally in a bench-scale crossflow-membrane filtration system, and compared with biofilms developing under identical conditions using unmodified spacers. In order to gain insight into the spatial distribution of silver ions in the spacer-filled channel, as well as the projected rate of release, numerical simulations of the channel hydrodynamics and ion transport were performed.

2. Model formulation

A computational model was developed with the goal of evaluating the effect of channel hydrodynamics on the distribution of silver ions released from the spacer. In particular, the calculations were used to examine the silver concentration on the membrane surface and the rate of release, the former impacting the envisioned bio-suppressive effect and the latter, determining the projected life-time of the spacer. The computational domain used was a 2D parallel-plate configuration, bounded by upper and lower permeable walls (the membranes) and with various spacer arrangements as illustrated in Fig. 1 (zigzag, submerged and cavity,

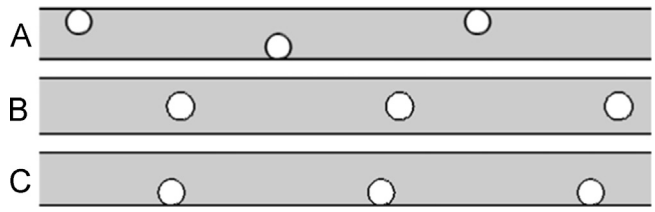

Fig. 1. Cross section configurations of the feed spacer channel considered in the computational model: (A) zigzag; (B) submerged; (C) cavity.

representing different sections of a 3D spacer [37,38]). The 2D model offers a significant computational advantage and, since the goal here was to gain physical insight, offers a simplified and intuitive view of the process, which is expected to qualitatively share the features of the realistic 3D case. However, it should be noted that this is only expected as long as the flow is stable, since the onset of instability creates a complex three-dimensional velocity field that features both longitudinal and transverse vortical structures [37,39]. The assumption of a steady-state laminar flow is normally justifiable at the Reynolds numbers (Re ≈ 100–200) used in the simulations and in actual flow-through experiments.

2.1. Model equations

2.1.1. Velocity and concentration field

The velocity field is described by the equations of motion for an incompressible fluid and the continuity equation, along with the advection-diffusion equation describing the solute transport:

$$\rho(\mathbf{u}\cdot\nabla)\mathbf{u} = -\nabla p + \nabla\cdot(\eta\nabla\mathbf{u})$$
$$\nabla.\mathbf{u} = 0 \quad (1)$$

$$\mathbf{u}\cdot\nabla c = \nabla\cdot(D\nabla c), \quad (2)$$

where $\mathbf{u}$ is the velocity vector, p is the pressure, ρ is the liquid density and η is the liquid dynamic viscosity.

2.1.2. Boundary conditions

For the velocity field, the following boundary conditions were imposed. At the inlet, a fully developed laminar velocity profile was specified, while the outflow boundary was set to constant (atmospheric) pressure. At the upper and lower boundaries (membrane surfaces) the tangential velocity was set to zero (no-slip condition) while the vertical component was set to a constant value corresponding with the experimentally determined value. Both velocity components were set to zero at the spacer-fluid interface.

The boundary conditions specified for the advection–diffusion equation, describing the silver ion concentration field in the channel, were as follows. At outlet boundary, as well as at the fluid-membrane interface, a zero concentration gradient was imposed; for the outlet, this is due to the assumption that it is advection-dominated, while the membranes were simply assumed to be fully retentive. The concentration in the inlet boundary was defined as zero as well as no ions were assumed to enter the channel. The spacer filaments were taken as sources of ions, hence a constant concentration was ascribed on the surface of the spacer. This corresponds to the case of a diffusion-limited heterogeneous reaction (i.e., fast kinetics).

Once the velocity and concentration fields were computed, for each spacer configuration, the total ion flux from a single spacer unit was found through integration of the local diffusive flux:

$$J = D\nabla c\cdot\mathbf{n}, \quad (3)$$

where $\mathbf{n}$ denotes the normal vector at the spacer-fluid interface. The life span of the spacer was then evaluated by equating the ion flux, taken here to be the constant rate of release, J, to the change

in the mass of silver on the spacer, $dm/dt = -J$, which predicts a linear decrease in silver loading with time, and from which the time to exhaustion of the silver ions can be found.

2.1.3. Computational details

The model equations were solved using a commercial finite-element package (Comsol Multiphysics v4.3). The computational domain was meshed using a structured, boundary-layer type mesh, with an increasing mesh density near the spacer and membranes surface. This enabled an efficient computation while retaining accuracy where the largest concentration variations were expected in the system. Mesh refinement was carried out to ensure the independence of the solution on the mesh. In all simulations, the channel length was defined as 2×10^{-2} m, channel height as 10^{-3} m, the fluid density and dynamic viscosity were taken as 1000 kg m^{-g}, and10^{-3} Pa s, respectively, and the silver ion diffusion coefficient D as 10^{-9} m^2 s^{-1}.

3. Experimental

3.1. Outline

The experimental work includes evaluation of the physical properties of the modified spacer by high resolution-scanning electron microscopy (HRSEM). The ability of the modified spacers to repress biofilm development on membranes was examined in flow-through cells designed to simulate the flow conditions in commercial spiral wound modules as previously described by Ronen et al. [19]. Flow cells included polysulfone ultrafiltration membranes for simplicity. Biofilm formation was promoted using a mixed microbial culture. Biofilm development on membranes and spacers was imaged by electron microscopy and confocal laser scanning microscopy (CLSM). Permeate flux was tracked during flow experiments as an indicator of membrane fouling at a constant pressure.

3.2. Materials

All chemicals were used without further purification. Luria-Bertani (LB) broth (Sigma) was used for maintenance and inoculum preparation (incubated for 24 h at 30 °C in shaken flasks). Antibacterial activity under static conditions were performed using *Pseudomonas putida* S-12 (ATCC 700801) as the model organism [5]. Flow experiments were performed using a mixed bacterial culture enriched from a continuous pilot plant membrane bioreactor (Zenon) running on domestic wastewater at the Technion campus [40] by successive cultivation in synthetic tertiary effluents medium [4].

3.2.1. Feed spacer modification with nanosilver

Modification of the spacers was done by sonochemical deposition at conditions similar to those described by Perkas et al. [31] and Ronen et al. [19]. Briefly, cleaned samples were immersed in 0.04 M silver nitrate solution with 10% [v/v] ethylene glycol, 90% DI (deionized) water. An aqueous solution of 24% ammonium hydroxide was added dropwise to the reaction slurry during the first 3 min of sonication. Samples were ultrasonicated for 180 min (100% intensity) using an ultrasonic horn tip (Vibra Cell 130, 20 KHz) at a controlled temperature of about 15 °C using a cooling bath. After modification, the spacers were first washed thoroughly with deionized water to remove traces of ammonia, and then with ethanol. Modified spacers were dried overnight at room temperature. Silver coating coverage was assesed by image analysis of HRSEM images (ImageJ v.1.46r) and silver loading was determined by gravimetric analysis.

3.2.2. Antibacterial activity measurements under static and flow conditions

The antibacterial potential of the modified feed spacer was evaluated under static and flow conditions as described by Ronen et al. [18,19]. Static tests were performed to provide evidence of the antibacterial activity of the modified spacers.

Static conditions tests were done by direct contact of a bacterial suspension. Sections of the modified spacer and unmodified spacer (2 cm × 2 cm) were placed in direct contact with saline containing a suspension of *P. putida* S-12. Samples were placed in an orbital shaker (100 rpm) for up to 6 h to ensure contact. Samples of the liquid were extracted at specific time points, diluted in triplicate and plated for viable cell counting on LB agar-medium [7,19]. The antibacterial potential of the spacer was determined as percentage of reduction between the initial and the time dependent viable cells counts.

Experiments under flow conditions were performed in dual-channel flow-through membrane cell system with internal recirculation operating in a continuous mode, one carrying the modified spacer and the other the unmodified spacer as control. The flow cells were equipped with a feed spacer on top of a membrane mimicking the flow conditions in a spiral-wound module. Flat sheet polysulfone membranes of 200 kDa molecular weight cut off (MWCO) (ymersp3001, GE Osmonics) were used for simplicity. The system was run under conditions comparable to field operation with continuous inoculation of a mixed enriched microbial population and typical tertiary total organic carbon (TOC) concentration. Feedwater consisted of sterile synthetic tertiary effluents [4] diluted in place with filtered tap water (0.8/0.2 μm filter, Pall) to a final TOC concentration of about 10 mg L^{-1}. The average bacterial concentration in the feed was kept constant (10^3–10^4 CFU mL^{-1}). The system operated at a constant pressure of 10 psi (~69 kPa) and a linear flPa velocity of about 0.15 ms^1 which is representative of typical spiral wound practice in commercial scale [8]. Permeate flux was manually measured every several hours, initial flux was 37 ± 1.47 LMH (2.5 ± 0.1 L m^{-2} h^{-1} per psi and inlet pressure was maintained at approximately 10 psi). Experiments duration was 230 h (~10 days). At the end of the experiments, the spacers and membranes were removed, thoroughly washed with a sterile saline (10 mL) solution and taken for further visualization and analysis.

3.2.3. Imaging methods

CLSM and HRSEM Images of the autopsied membranes and spacers were taken from at least 8 random areas on the surface. The displayed images are representative images.

3.2.3.1. Feed spacer. Analysis of modified and unmodified spacers before flow experiments was performed using HRSEM (Carl Zeiss Ultra plus HRSEM 1 kV). Prior to imaging, samples were washed with deionized water and ethanol and air dried at room temperature overnight.

3.2.3.2. Biofilm development. Biofilm presence and development on membranes were evaluated by HRSEM as described by Ronen et al. [19]. Samples were washed and fixed using 2.5% (v/v) glutaraldehyde, dehydrated using an ethanol gradient in the cold and dried in the ambient before imaging. Biofilm viability was estimated using a Carl Zeiss CLSM (LSM 510 META) with an Apo 60 × 1.40 objective. Dead-live bacteria visualization was done by staining using propidium iodide at a concentration of 30 μM (P4170; Sigma) and 5-cyano-2,3-ditolyl tetrazolium chloride at a concentration of 30 mM (CTC, *B34956, Invitrogen*-Molecular Probes). Staining concentrations and exposure were based on literature [5,41].

3.2.4. Image processing and evaluation of biofilm

The area covered by attached bacteria was estimated using imaging analysis program (ImageJ v.1.46r). Analysis method was based on literature and guidance for evaluating bacteria cell numbers [42] and modified to estimate their total area. Imaris 7.6.1 (Bitplane) was used for dead-live analysis of CLSM images. Images were processed to include all z-sections and flattened to a single overlaying layer.

3.2.5. Assessment of bacteria concentration by TOC measurements

Concentration of the bacteria attached to the membranes was evacuated by TOC measurement (TOC-V series, Shimadzu). Section of the membranes (1.5 cm^2) were cut and placed in a 4.5 mL sterile saline containing 0.5% w/w tween−80 and 2.5 g of sterile glass beads. Samples were vortexed for 40 s and afterwards the solution was tested for TOC concentration. Experiments were repeated at least thrice. Bacteria concentration was estimated by considering a single bacterial cell of spherical shape of approximately 1 μm diameter and 1.03 g cm^{-3} density. The estimated cell volume will be 0.52×10^{-12} cm^3 and the cell mass will be 0.54×10^{-12} g per cell. Considering that approximately 30% of the cell weight is dry material and containing 90% organic material of which approximately 58% is C, the amount of organic carbon per cell comes to 8.5×10^{-12} μg C per cell.

3.2.6. Silver leaching tests

Silver leaching is an important factor influencing the potential activity of the modified spacer and its life span. Leaching was tested in several water matrix which represent typical working and cleaning conditions, such as deionized water, synthetic seawater, acidic and basic water solutions (pH=2 and pH=13, respectively). Sections of the spacer (1 cm^2) were immersed in 50 mL of the tested solutions for seven and 14 days at room temperature [43]. To ensure mixing and contact, the samples were shaken at 150 rpm during the length of the tests. At several time points, the solutions were sampled and silver concentration was determined by inductive coupled plasma (ICP).

4. Results

4.1. Characterization of the nanosilver-modified spacers

The modified spacers turned black due to the silver coating on the surface of the polypropylene (Fig. 1S), in line with previous reports regarding nanosilver embedment by sonochemical deposition on polymers and cotton [44]. Characterization of the spacers was first performed through imaging by HRSEM (Fig. 2). The unmodified spacer surface shows a single, low density component, typical for a carbon-based material such as polypropylene (Fig. 2A). The influence of the sonochemical deposition is observed as white patches on the spacer surface (Fig. 2B and C) – these represent a material with higher electron density compared with the polymer background, such as metals or metal oxides. Calculation of the area coated by silver using image processing of the secondary electron (SE) imaging indicated 90–99% surface coating (Fig. 2B). Backscattered secondary electron (BSE) imaging indicates that most of the particles on the polypropylene surface are nano-sized with fewer, larger particles (Fig. 2C). Silver loading was estimated by gravimetric analysis to be 9% w/w.

Leaching of silver ions from the modified spacers was evaluated next. The release of silver ions is related to the life span spacer. Leaching from the modified spacer was assessed under equilibrium conditions against deionized water, synthetic seawater, as well as acidic and basic (pH of 3 and 12 relatively) solutions. Samples were taken after seven and 14 days (Table 1). Results indicate that a small concentration of silver was released to the solution after 7 and 14 days in all water matrixes leading to the conclusion that the leaching is quite small. Silver leaching was at an average rate of 0.013 ± 0.008 mg L^{-1} per day on deionized water, 0.022 ± 0.005 mg L^{-1} per day on synthetic seawater, a higher rate of about 0.033 ± 0.005 mg L^{-1} per day for basic water solutions (pH 12) and a negligible concentration of 0.002 ± 0.001 mg L^{-1} per day for acidic water solutions (pH 3). Based on these characteristics, it is estimated that silver is released at a rate of 0.003–0.04% w/w per day. Therefore, a modified spacer with 9% w/w silver loading should suffice for the predicted life span of the membrane module under the current conditions. Since silver

Table 1
Leaching of silver ions from the nanosilver-modified spacers.

Water matrix	Dissolved silver concentration (mg L^{-1})			Average daily weight loss (%)
	After 7 days	After 14 days	Average daily leaching	
Deionized water	0.078 ± 0.005	0.106 ± 0.008	0.013	0.016
Synthetic seawater	0.177 ± 0.001	0.128 ± 0.005	0.022	0.028
pH=3	<0.02	0.025 ± 0.002	0.002	0.003
pH=12	0.243 ± 0.08	0.263 ± 0.05	0.033	0.041

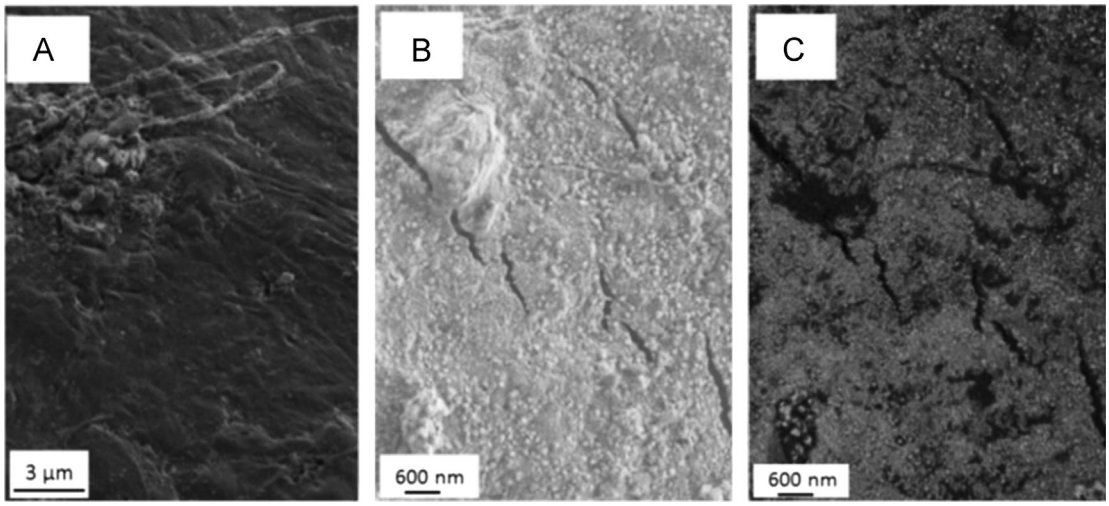

Fig. 2. HRSEM micrographs of the polypropylene feed spacers. (A) Unmodified spacer (magnification ×10 K). (B) Surface of the nanosilver modified spacer, SE detector (magnification ×20 K); (C) Surface of the nanosilver modified spacer, BSE detector. Dark area represents polypropylene and bright area represents silver nanoparticles.

ions are expected to be largely rejected by the RO membrane, they should not pose any significant health threat. EPA secondary drinking guidelines recommend a relatively low concentration limit for silver in water (≤ 0.1 mg L^{-1}) [45].

The antibacterial properties of the modified spacers was determined in static liquid cultures following 1,2,3 and 6 h of direct contact (Table 2). An affective bacterial reduction was seen even after 1 h of direct contact (93% reduction) compared with no reduction observed in the control samples. Practically complete bacterial reduction (8-logs) was observed after 3 h, compared with a 40–55% reduction in the control. All control samples showed a reduction of up to 50% after 6 h due to natural bacterial decay as assessed by viable cell plating.

4.2. Antibiofouling activity of the modified spacer under crossflow conditions

Flow experiments under conditions comparable to field operation (~ 10 mg L^{-1} TOC and 10^3–10^4 CFU mL^{-1} bacterial concentration in the feedwater) were performed to evaluate the antibiofouling capabilities of the modified spacers. Daily samples were taken for enumeration of planktonic bacteria, after 230 h of experiment the cells were dismantled, and the membranes and spacers autopsied. Fig. 3 shows HRSEM micrographs of the autopsied membranes adjacent to the spacers. The membrane near the unmodified spacer displayed a developed biofilm structure covering almost all the surface area (Fig. 3, panels A and C). In contrast, the membrane adjacent to the modified spacer displayed only small patches of attached bacteria in a monolayer structure (Fig. 3, panels B and D). The area coverage of the biofilm was estimated to be approximately 87.2% and 2.4%, on the membranes adjacent to the unmodified spacer and modified spacer, respectively (see Fig. 2S for analysis procedure). These results clearly indicate a high antibiofouling potential of the modified spacers. Biofilms developed in a multilayer structure while area coverage was evaluated by 2D imaging, therefore, additional semi-empirical estimation of bacteria concentration on the membranes was performed based on TOC measurements. The average bacteria concentration calculated was 260 ± 8.6 and 13 ± 12.5 cells per 100 μm^2 for the control and treatment, respectively, in line the estimated area coverage. Overall, the membrane near the modified spacer exhibited 10–20 folds less attached bacteria per area than the control membrane.

In addition to bacteria concentration and surface coverage, dead/live staining and imaging by CLSM was performed (Fig. 4). Dead bacteria were stained by PI and live bacteria were stained by CTC. Estimation of the attached cells was done using image analysis (Imaris software) which distinguishes between individual cells (Table 3). It can generally be seen that the membrane near the unmodified spacer exhibited large clusters of bacteria, most of which were alive (12% dead). In contrast, the membrane near the modified spacer showed significantly less bacteria attached to the surface, of which 27% were dead.

Fig. 5 presents the measured permeate flux vs. time for multiple experiments. An intrinsic self-decrease of permeability was observed for approximately 3 days until the system stabilized. After 10 days of flow, the permeate flux of the membrane with the modified spacer was almost 5-fold higher (about a 45% flux decline) than that obtained

Table 2
Antibacterial activity test against *P. putida* S12 in static liquid cultures.

Sample[a]	Survival fraction (%)			
	1 h	2 h	3 h	6 h
Control saline	100	76	60	53
Unmodified spacer	100	70	45	45
Modified spacer	7	3	ND[b]	ND[b]

[a] Initial bacteria concentration was about 10^8 CFU mL^{-1} in saline.
[b] ND: not detectable.

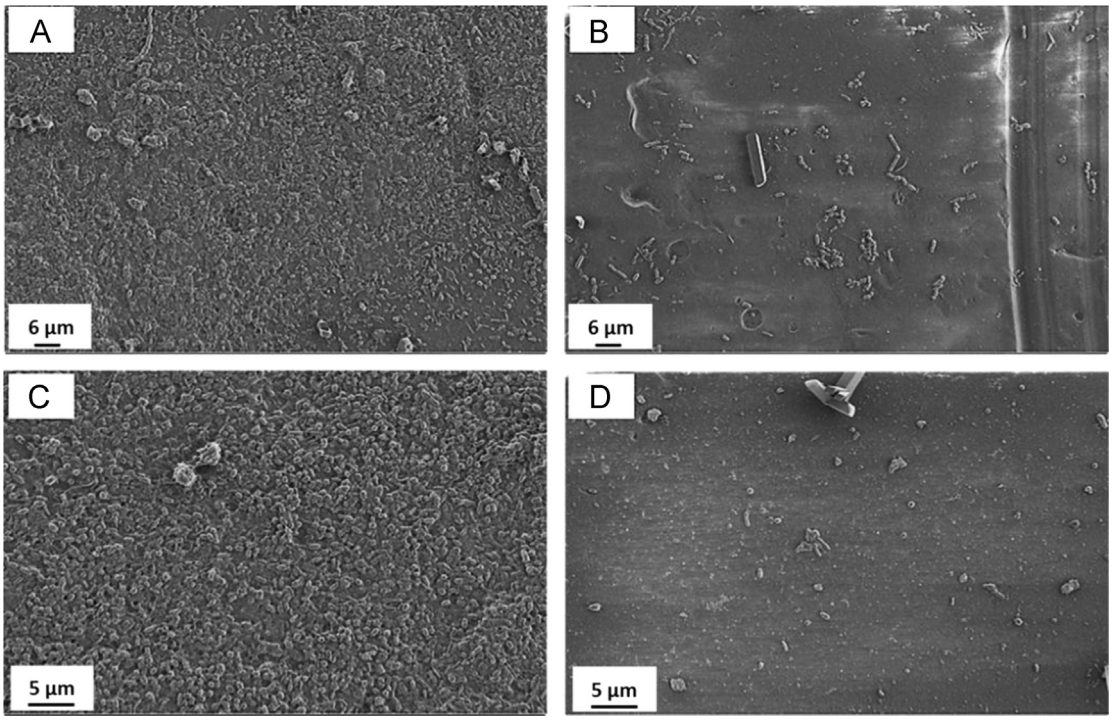

Fig. 3. HRSEM micrographs of 200 kDa polysulfone ultrafiltration membrane adjacent to spacers after 230 h of exposure to flow with 10^4 CFU mL^{-1} mixed bacterial culture. Left: membrane adjacent to unmodified spacer (control); Right: membrane adjacent to modified spacer (treatment). A,B: $\times 3$ K magnification; C,D: $\times 5$ K magnification. Estimated concentration of bacteria attached per membrane area calculated by TOC measurement was 260 ± 8.6 and 13 ± 12.5 cells per 100 μm^2 for the control and treatment, respectively.

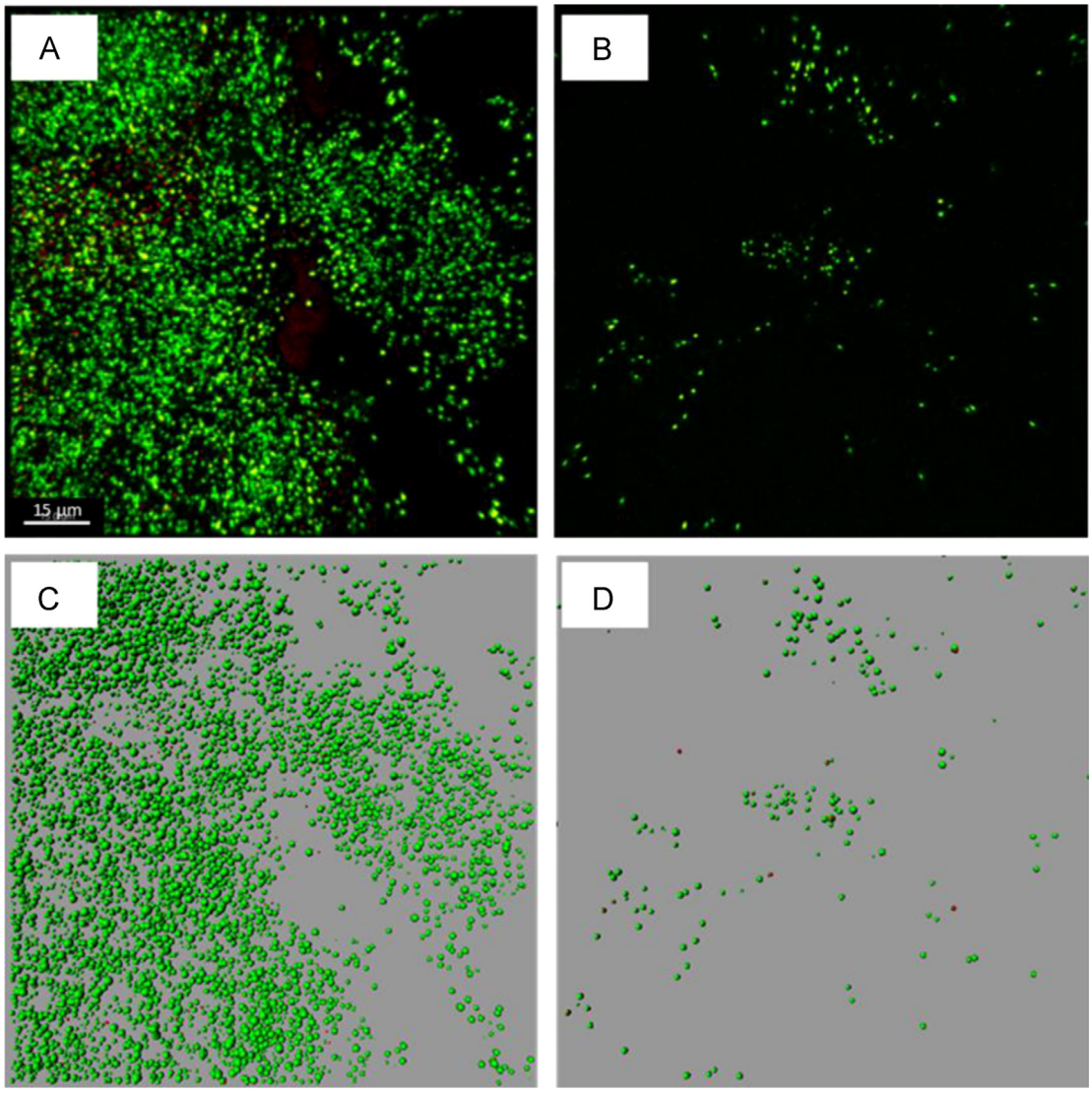

Fig. 4. CLSM imaging of a 200 kDa polysulfone ultrafiltration membrane after 230 h of exposure to flow with 10^4 CFU mL^{-1} mixed bacterial cultures with an adjacent spacer. Top: CLSM images; Bottom: imaris software analysis of CLSM images. A,C: membrane adjacent to unmodified spacer; B,D: membrane adjacent to modified spacer. Live cells are stained in green (CTC) and dead cells in red (PI). (For interpretation of the references to color in this figure legend, the reader is referred to the web version of this article.)

Table 3
Estimation of dead/live attached bacteria on the membrane by CLSM.

Spacer	Live bacteria	Dead bacteria	Dead/Live	Dead/Total
	(Cells/100 μm^2)		(%)	
Unmodified (control)	2525 ± 180	354 ± 74.8	14	12
Modified	248 ± 98	92 ± 61	37	27

with the unmodified spacer, (90% decline). The change in permeate flux during the experiments can be mainly attributed to the deposition of bacteria and biofilm development on the membranes. Images of the membranes and spacers at the end of the experiment are presented in the insets of Fig. 5. A thick 'gel' biofilm layer can be seen on top of the membrane near the unmodified spacer while significantly less biofilm can be seen on the membrane adjacent to the modified spacer.

4.3. Numerical simulation of velocity field and silver ions distribution

Representative plots of the velocity field, obtained by the numerical simulation of the flow near and around spacers with three possible configurations are presented in Fig. 6 (top panel). The spacer decreases the available area for flow, and therefore, the velocity above and below the spacer increases in the submerged configuration. In the zigzag and cavity configurations the flow velocity increased opposite to the spacer's location and significantly decreased near the spacer, thus, increasing stagnation points and low flow velocities near the membrane surface, these results are in correlation with the literature regarding the spacers' hydrodynamic influence in a narrow channel [46].

The distribution of silver ions released from the spacer along the feed channel is presented in Fig. 6 (bottom panel). Simulations indicate that a high concentration of silver ions is found in the areas with low flow velocities near the spacers in the cavity and zigzag configurations while the areas which were subjected to higher flow velocities corresponded with low silver ion concentrations, these results correspond with simulations done by Schwinge et al. [47] which showed the influence of spacer configurations on mass transfer from the membrane walls, indicating a relatively low mass transfer at low Reynolds numbers and therefore maintaining a high concentration near the membrane.

Silver ion concentrations were evaluated near the upper membrane surface for both cavity and zigzag configurations (Fig. 7), as the

concentration near the membrane has significant influence on the antibacterial capacity of the spacer. Results indicate that for the cavity configuration, 50% of the spacer-interface concentration is reached near the upper membrane after about 1.2 cm of flow (~3 repeating units of spacer). In the zigzag configuration only 35% is reached at the same distance but the opposite membrane is affected as well. Overall, the silver concentration near the membrane is relatively high after a short distance. It should be noted that the modified spacer used for the experiments was significantly longer than the simulated flow channel (~80 mm). As spacer units are placed about 4 mm from each other, the experimental system was based on more than 20 continuous spacer units.

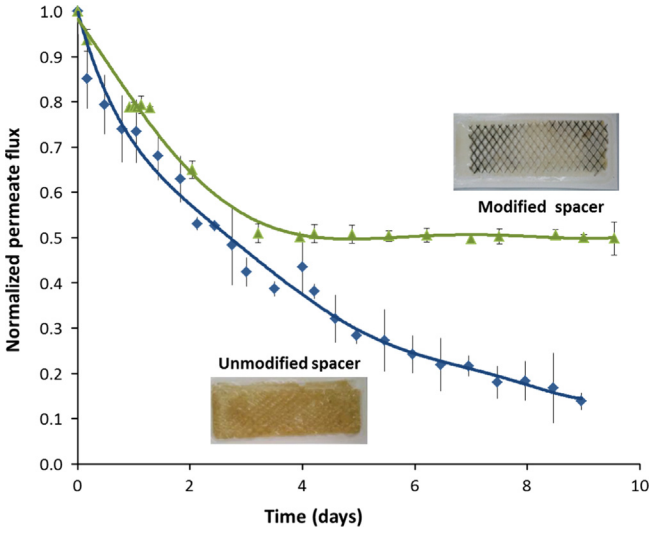

Fig. 5. Mean flux profile of the 200 kDa polysulfone membrane during a 230 h flow experiment in a planar flow cell with exposure to 10^4 CFU mL^{-1} mixed bacterial cultures. Initial permeability was 2.5 ± 0.1 L m^{-2} h^{-1} per psi and inlet pressure was maintained at approximately 10 psi. Insets show a close-up view of the respective spacers at the end of the experiments.

The silver ion flux (in mole/s), released from the spacer, was calculated per single unit of the spacer (taken as a cylinder with a radius of 2.5 mm) as a function of the crossflow velocity (0.01–0.15 ms^{-1}). The ion flux was calculated for the third unit of spacer in the flow channel as this spacer unit simulates developed hydrodynamic conditions (in the periodic sense) while also accounting for the influence of the silver ions released from the previous spacer units (see Fig. 4S) [47]. Simulations indicate that ions flux is influenced by the concentration gradient near the spacer, and therefore, the flux increases with correlation to the crossflow velocity in the channel (see Fig. 3S). Furthermore, the lowest flux was found for the cavity configuration and the highest values were obtained for the zigzag configuration as it is subjected to a lower concentration of silver ions from the previous spacer units.

5. Discussion

The morphology of the modified spacers reported here is in line with results described in the literature regarding silver sonochemical deposition and surface modification of polymers [31–34,36,45]. Moreover, although the deposited nanoparticles size can vary as a function of sonochemical duration, intensity, solution concentration and additives, in general, the surface coating was uniform and particles were in the nano-scale size range.

Ion leaching experiments showed a small concentration of silver leaching from the modified spacer in all water media, suggesting that the sonochemically deposited nanosilver is strongly anchored to the spacer. These results are in correlation with Perelshtein et al. [36] which tested the stability of nanosilver coated fibers by up to 20 washing cycles in hot water (40 °C) indicating negligible leaching of silver. Furthermore, they showed on several polymers and fibers that the coating is a physical adsorption of the nanoparticles on the substrate as a result of the sonication. The embedment of the nanoparticles is derived from the migration of the nanosilver particles towards the surface at a very high velocity. This phenomenon is induced by the

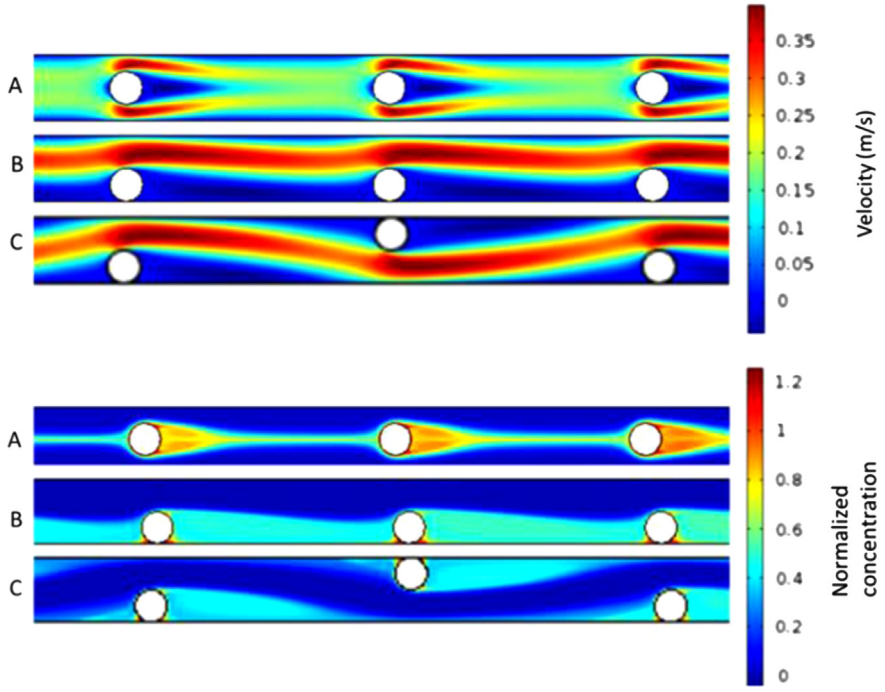

Fig. 6. Velocity field and silver ions distribution as a function of spacer configuration obtained by the numerical simulation of the flow near and around spacers. Top: flow velocity distributions. Bottom: silver ions concentration distributions. Spacer configurations: A-submerged, B-cavity, and C-zigzag. Concentrations are scaled by the concentration at the spacer-liquid interface.

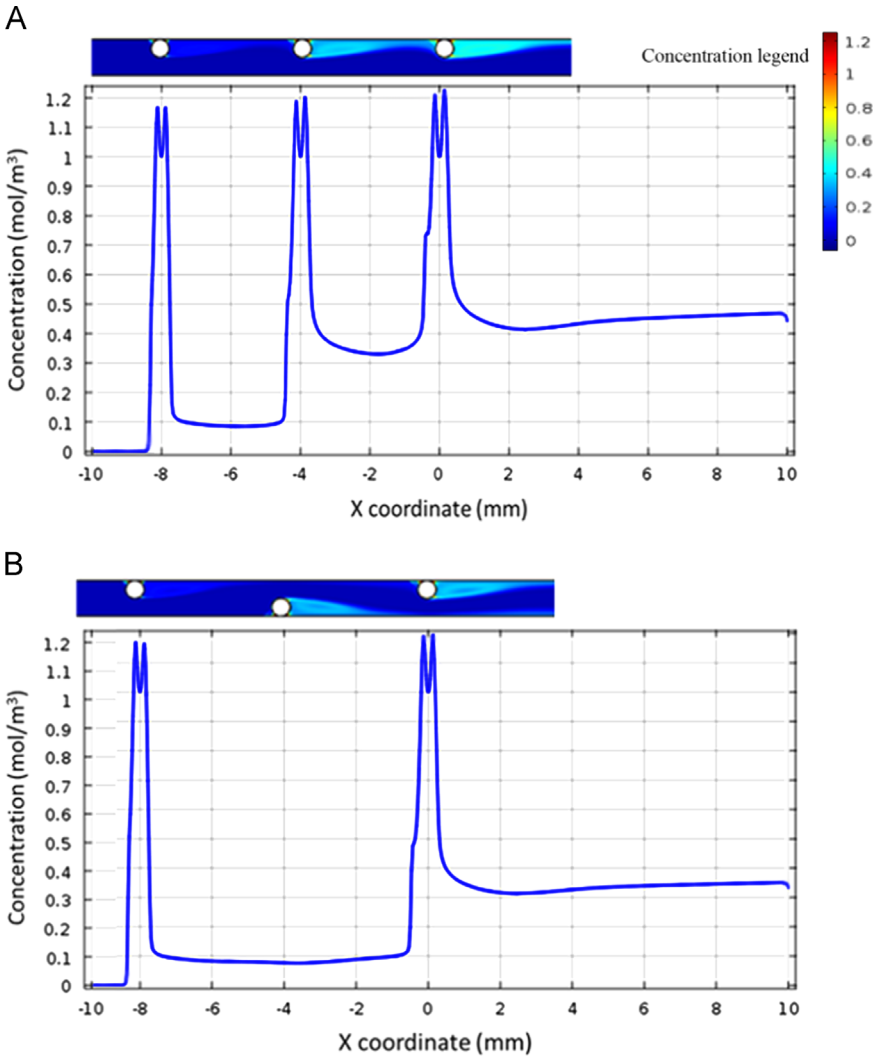

Fig. 7. Silver ions concentration profile near the upper membrane. Top: concentration gradients in the flow channel. Bottom: concentration profile near the membrane. A-cavity, and B-zigzag.

influence of the sonochemical irradiation on the water which causes cavitation and heating, resulting in a local melting of the surface, which may be the reason why the particles strongly adhere to the sample [48]. In addition, our leaching results indicated that the silver ion concentrations in all water media are an order of magnitude lower than the EPA secondary drinking water regulations [45], thus, they are not considered harmful to the environment. Previous reports showed nanosilver loading by sonochemical deposition of up to 7.5% w/w depending on deposition duration, intensity and solution concentration [31–34,36,44]. In our case, 9% w/w loading was achieved as measured by gravimetric methods due to increased sonochemical duration (3 h) which was repeated per small sections of the spacer. It should be noted that coating occurs mainly on the upper layer of the sample meaning a high active concentration on the surface.

The antibacterial effect of the modified spacer is in line with other silver-coated surfaces. Perelshtein et al. [36] showed that when using polymer fabrics (nylon, polyester and cotton), the addition of 1% w/w of nano silver led to the reduction of most bacteria in 1 h and all bacteria after 2 h. In our case, the modified spacer had a higher loading of nanosilver but a lower active surface area compared with fibers, thus, leading to a high reduction after 1 h and a complete reduction after 3 h.

The antibacterial ability of nanosilver measured by their minimum inhibitory concentration (MIC) in a solution, was reported to be small ($\sim$2 nM or 2.14×10^{-4} mg L^{-1}) [49]. Silver concentrations found in our batch tests under static conditions were higher than the MIC concentration (about 0.02 mg L^{-1}) and therefore highly effective in bacteria reduction. Experiments performed in flow regime were designed to simulate 'real life' conditions such as the inflow of RO membrane with tertiary effluents. Tertiary effluents have a typical bacteria concentration of about 10^3 CFU mL^{-1} and TOC values of about approximately 10–13 mg L^{-1}. Pretreated seawater for desalination has a similar bacteria concentration (or even less) with much lower TOC values [50]. To increase biofilm formation in the frame of time studied, the inflow concentration in our work included about 10^4 CFU mL^{-1} and 10 mg L^{-1}. In addition, whereas in a practical system, organic carbon is only partially available for bacteria, the feed applied in our experiments included a highly available carbon source. Exposure of the flow system to these conditions was done to maximize bacterial growth and show the modified spacer's ability to cope with increased biofilm formation.

Both HRSEM and CLSM images confirmed the decrease for bacteria in the presence of the modified spacer. While the membrane adjacent to the unmodified spacer showed a developed biofilm layer with a thickness of 10–15 μm, the membrane adjacent to the modified spacer displayed only few patches of attached bacteria as sporadic cells and none of the bacteria groups can be defined as a developed biofilm layer. CLSM images showed that a higher percentage of the bacteria on the membrane adjacent

to the modified spacer were found inactive or dead compared with the control. These results reflect on a very active antibacterial effect of the nanosilver. Bacteria assessment via TOC measurement and image analysis show a similar trend, which highlights the modified spacer's ability to decrease bacterial attachment during flow conditions. As the permeate flux profile is a good indication of the biofouling severity, the permeate flux of the membrane adjacent to the modified spacer was almost 5-folds higher than that of the membrane adjacent to the unmodified spacer, with a net decrease of about 50% compared with 90% relatively. These changes in permeate flux can be mainly attributed to the deposition of a developed biofilm layer on the membrane adjacent to the unmodified spacer. We cannot rule out that recirculation may eventually lead to some increase of silver ions concentration in the flow cell as compared to single pass conditions. However, since the hydraulic retention time in the feed bioreactor was set to be less than the doubling time of the model bacterium, the continuous inflow of fresh solution to the reactor diluted the silver ions concentration as washed out planktonic cells. In addition, since a constant feed concentration of bacteria was applied, the ratio of silver to bacteria would be roughly constant along the runs.

Two additional factors should be taken into consideration. It should be noted that fouling rate increases with permeate flux through the membrane, as higher flux increases the transport of bacteria and nutrients towards the membrane surface [5]. As our system was designed to maintain a constant pressure, the flux through the membrane adjacent to the modified spacer was kept relatively high compared with the control system, therefore it should have been subjected to a potentially high fouling rate. This paradigmatic flux/fouling relationship emphasizes even more the high efficiency of the modified spacer to control biofilm development on the membrane. Furthermore, the flow experiments presented here were performed using a mixed bacterial culture, which represents harsher conditions as the interaction between bacteria species could potentially increase biofilm development.

Simulations showed the spatial distribution of flow velocities and silver ions from the spacer at several possible configurations. Each configuration represents a cross section of the membrane module in a different area, resulting in specific flow channel geometry. The zigzag and cavity configuration displayed high flow velocities opposite to the spacer unit and low flow velocities near the spacer and downstream, leading to a decreased flow velocity and therefore low shear forces and stagnation points, which are prone for bacterial attachment and biofouling. Simulation indicates that silver ions concentration in these configurations was relatively high near the spacer and the adjacent membrane. Silver ions concentration reached about 50% of the initial normalized value after about 3 spacer units. In contrast, the simulation regarding the submerged configuration did not display silver ions on the membrane surface. Nevertheless, the flow velocities near the upper and lower boundaries of the flow channel (membranes) were relatively high which could increase the shear on the membranes and decreases particles and bacterial attachment.

In the simulations regarding the zigzag and submerged configurations, silver ions concentration near the spacer units increased as a function of increasing spacer units and length. It could be assumed that the high ion concentrations found near the membranes could influence the approximate bacteria cells in water stream and prevent the development of a biofilm from the bacterial cells which are driven towards the membrane by the permeation flux.

6. Conclusions

Silver ions release from the spacer, simulated by numerical modeling showed that silver ions were present at high concentrations throughout the flow channel as a function of the spacer's spatial configuration. Higher concentrations of silver ions were found near the membrane surface in the zigzag and cavity configurations. The ions presence may prevent bacteria attachment and biofilm development near the stagnation points caused by the spacers and near the adjacent membranes.

As for the experimental section, modification of the spacer was done by sonochemical deposition of nanosilver, which is considered highly antibacterial active compared with silver micro-particles due to their high surface area to volume. Silver ion leaching from the modified spacer was low but still the detected concentrations were higher than the MIC values for nanosilver in the literature. Flow-through experiments were performed using mixed cultures under conditions simulating RO treatment of tertiary effluents. Experiments duration was about 10 days, which is a sufficient time to determine biofilm development and membrane clogging. Biofilm development on a membrane operating in crossflow mode could be controlled by means of a nanosilver modified spacer with proven antibacterial qualities. Apparently, the modified spacer influenced bacteria cell not only in direct contact with the modified spacer but throughout the flow channel. This effect was also observed in the numerical simulations as an increase in silver ions concentration along the membrane surface. The life span of the modified spacer was estimated taking into account diffusion in a flowing field as governing mechanism, whereas leaching experiments were performed under equilibrium conditions. This issue requires further consideration in future work.

Although the results are encouraging, we cannot neglect the possibility of mutation and interspecies gene flow leading to silver resistant bacteria in long-term flow runs with the modified spacer [51,52]. Therefore, it is well understood that effective biofilm prevention is not a single step solution and should be done by using an integrated approach [53], but an effective antibacterial spacer could be part of the solution.

Acknowledgments

This work was partially funded by the Russell Berrie Nanotechnology Institute (RBNI) at the Technion. The generous financial support of the Grand Water Research Institute and the Rieger Foundation is gratefully acknowledged.

Appendix A. Supporting information

Supplementary data associated with this article can be found in the online version at http://dx.doi.org/10.1016/j.memsci.2014.10.042.

References

[1] A.M. Comerton, R.C. Andrews, D.M. Bagley, Evaluation of an MBR-RO system to produce high quality reuse water: microbial control, DBP formation and nitrate, Water Res. 39 (2005) 3982–3990.
[2] H.C. Flemming, G. Schaule, T. Griebe, J. Schmitt, A. Tamachkiarowa, Biofouling—the Achilles heel of membrane processes, Desalination 113 (1997) 215–225.
[3] J. Gutman, S.L. Walker, V. Freger, M. Herzberg, Bacterial attachment and viscoelasticity: physicochemical and motility effects analyzed using quartz crystal microbalance with dissipation (QCM-D), Environ. Sci. Technol. 47 (2013) 398–404.
[4] M. Herzberg, M. Elimelech, Biofouling of reverse osmosis membranes: role of biofilm-enhanced osmotic pressure, J. Membr. Sci. 295 (2007) 11–20.
[5] L. Eshed, S. Yaron, C.G. Dosoretz, Effect of permeate drag force on the development of a biofouling layer in a pressure-driven membrane separation system, Appl. Environ. Microbiol. 74 (2008) 7338–7347.
[6] H. Ivnitsky, I. Katz, D. Minz, E. Shimoni, Y. Chen, J. Tarchitzky, R. Semiat, C.G. Dosoretz, Characterization of membrane biofouling in nanofiltration processes of wastewater treatment, Desalination 185 (2005) 255–268.
[7] H. Ivnitsky, I. Katz, D. Minz, G. Volvovic, E. Shimoni, E. Kesselman, R. Semiat, C.G. Dosoretz, Bacterial community composition and structure of biofilms developing on nanofiltration membranes applied to wastewater treatment, Water Res. 41 (2007) 3924–3935.

[8] J.S. Vrouwenvelder, D.A. Graf von der Schulenburg, J.C. Kruithof, M.L. Johns, M.C.M. van Loosdrecht, Biofouling of spiral-wound nanofiltration and reverse osmosis membranes: a feed spacer problem, Water Res. 43 (2009) 583–594.
[9] H.L. Yang, J.C. Lin, C. Huang, Application of nanosilver surface modification to RO membrane and spacer for mitigating biofouling in seawater desalination, Water Res. 43 (2009) 3777–3786.
[10] P.A. Araújo, D.J. Miller, P.B. Correia, M.C.M. van Loosdrecht, J.C. Kruithof, B.D. Freeman, D.R. Paul, J.S. Vrouwenvelder, Impact of feed spacer and membrane modification by hydrophilic, bactericidal and biocidal coating on biofouling control, Desalination 295 (2012) 1–10.
[11] P.A. Araújo, J.C. Kruithof, M.C.M. Van Loosdrecht, J.S. Vrouwenvelder, The potential of standard and modified feed spacers for biofouling control, J. Membr. Sci. 403–404 (2012) 58–70.
[12] J.S. Vrouwenvelder, C. Picioreanu, J.C. Kruithof, M.C.M. van Loosdrecht, Biofouling in spiral wound membrane systems: three-dimensional CFD model based evaluation of experimental data, J. Membr. Sci 346 (2010) 71–85.
[13] C. Picioreanu, J.S. Vrouwenvelder, M.C.M. van Loosdrecht, Three-dimensional modeling of biofouling and fluid dynamics in feed spacer channels of membrane devices, J. Membr. Sci 345 (2009) 340–354.
[14] A.I. Radu, J.S. Vrouwenvelder, M.C.M. van Loosdrecht, C. Picioreanu, Modeling the effect of biofilm formation on reverse osmosis performance: flux, feed channel pressure drop and solute passage, J. Membr. Sci 365 (2010) 1–15.
[15] R. Franks, C. Bartels, A. Anit, Demonstrating improved RO system performence with new low differential (LD) technology, Hydranautics, CA.
[16] R. Hausman, T. Gullinkala, I.C. Escobar, Development of low-biofouling polypropylene feedspacers for reverse osmosis, Appl. Polym. Sci. 114 (2009) 3068–3073.
[17] D.J. Miller, P.A. Araújo, P.B. Correia, M.M. Ramsey, J.C. Kruithof, M.C.M. van Loosdrecht, B.D. Freeman, D.R. Paul, M. Whiteley, J.S. Vrouwenvelder, Short-term adhesion and long-term biofouling testing of polydopamine and poly (ethylene glycol) surface modifications of membranes and feed spacers for biofouling control, Water Res. 46 (2012) 3737–3753.
[18] A. Ronen, R. Semiat, C.G. Dosoretz, Antibacterial efficiency of composite nano-ZnO in biofilm development in flow-through systems, Desalin, Water Treat. 51 (2013) 988–996.
[19] A. Ronen, R. Semiat, C.G. Dosoretz, Impact of ZnO embedded feed spacer on biofilm development in membrane systems, Water Res. 47 (2013) 6628–6638.
[20] D.P. Dowling, K. Donnelly, M.L. McConnell, R. Eloy, M.N. Arnaud, Deposition of anti-bacterial silver coatings on polymeric substrates, Thin Solid Films 398–399 (2001) 602–606.
[21] C. Marambio-Jones, E.M.V. Hoek, A review of the antibacterial effects of silver nanomaterials and potential implications for human health and the environment, J. Nanoparticle Res. 12 (2010) 1531–1551.
[22] Q. Li, S. Mahendra, D.Y. Lyon, L. Brunet, M.V. Liga, Antimicrobial nanomaterials for water disinfection and microbial control: potential applications and implications, Water Res. 42 (2008) 4591–4602.
[23] V.A. Oyanedel-Craver, J.A. Smith, Sustainable colloidal-silver-impregnated ceramic filter for point-of-use water treatment, Environ. Sci. Technol. 42 (2008) 927–933.
[24] W.L. Chou, D.G. Yu, M.C. Yang, The preparation and characterization of silver-loading cellulose acetate hollow fiber membrane for water treatment, Polym. Adv. Technol. 16 (2005) 600–607.
[25] T.A. Dankovich, D.G. Gray, Bactericidal paper impregnated with silver nanoparticles for point-of-use water treatment, Environ. Sci. Technol. 45 (2011) 1992–1998.
[26] K.B. Holt, A.J. Bard, Interaction of silver(I) ions with the respiratory chain of *Escherichia coli*: an electrochemical and scanning electrochemical microscopy study of the antimicrobial mechanism of micromolar Ag+, Biochemistry 44 (2005) 13214–13223.
[27] S.Y. Liau, D.C. Read, W.J. Pugh, J.R. Furr, A.D. Russell, Interaction of silver nitrate with readily identifiable groups: relationship to the antibacterial action of silver ions, Lett. Appl. Microbiol. 25 (1997) 279–283.
[28] H.J. Park, J.Y. Kim, J. Kim, J.H. Lee, J.S. Hahn, M.B. Gu, J. Yoon, Silver-ion-mediated reactive oxygen species generation affecting bactericidal activity, Water Res. 43 (2009) 1027–1032.
[29] W.J. Jin, H.K. Lee, E.H. Jeong, W.H. Park, J.H. Youk, Preparation of polymer nanofibers containing silver nanoparticles by using poly(N-vinylpyrrolidone), Macromol. Rapid Commun. 26 (2005) 1903–1907.
[30] S.T. Dubas, P. Kumlangdudsana, P. Potiyaraj, Layer-by-layer deposition of antimicrobial silver nanoparticles on textile fibers, Colloids Surf. A: Physicochem. Eng. Asp. 289 (2006) 105–109.
[31] N. Perkas, G. Amirian, G. Applerot, E. Efendiev, Y. Kaganovskii, A.V. Ghule, B.J. Chen, Y.C. Ling, A. Gedanken, Depositing silver nanoparticles on/in a glass slide by the sonochemical method, Nanotechnology 19 (2008) 1–10.
[32] V.G. Pol, D.N. Srivastava, O. Palchik, V. Palchik, M.A. Slifkin, A.M. Weiss, A. Gedanken, Sonochemical deposition of silver nanoparticles on silica spheres, Langmuir 18 (2002) 3352–3357.
[33] L. Hadad, N. Perkas, Y. Gofer, J. Calderon-Moreno, A. Ghule, A. Gedanken, Sonochemical deposition of silver nanoparticles on wool fibers, J. Appl. Polym. Sci. 104 (2007) 1732–1737.
[34] M. Soloviev, A. Gedanken, Coating a stainless steel plate with silver nanoparticles by the sonochemical method, Ultrason. Sonochem. 18 (2011) 356–362.
[35] N. Perkas, M. Shuster, G. Amirian, Y. Koltypin, A. Gedanken, Sonochemical immobilization of silver nanoparticles on porous polypropylene, J. Polym. Sci. Part A: Polym. Chem. 46 (2008) 1719–1729.
[36] I. Perelshtein, G. Applerot, N. Perkas, G. Guibert, S. Mikhailov, A. Gedanken, Sonochemical coating of silver nanoparticles on textile fabrics (nylon, polyester and cotton) and their antibacterial activity, Nanotechnology 19 (2008) 1–7.
[37] J. Schwinge, D.E. Wiley, D.F. Fletcherb, A CFD, study of unsteady flow in narrow spacer-filled channels for spiral-wound membrane modules, Desalination 146 (2002) 195–201.
[38] A. Subramani, S. Kim, E.M.V. Hoek, Pressure, flow, and concentration profiles in open and spacer-filled membrane channels, J. Membr. Sci. 277 (2006) 7–17.
[39] A.L. Ahmad, K.K. Lau, M.Z. Abu Bakar, Impact of different spacer filament geometries on concentration polarization control in narrow membrane channel, J. Membr. Sci. 262 (2005) 138–152.
[40] I. Katz, C.G. Dosoretz, Desalination of domestic wastewater effluents: phosphate removal as pretreatment, Desalination 222 (2008) 230–242.
[41] V. Créach, A.C. Baudoux, G. Bertru, B. Le Rouzic, Direct estimate of active bacteria: CTC use and limitations, J. Microbiol. Methods 52 (2003) 19–28.
[42] C. Labno, Basic Intensity Quantification with ImageJ, Integrated Light Microscopy Core, University of Chicago.
[43] I.C. Escobar, T. Gullinkala, R. Hausman, Anti-Biofouling Materials and Methods of Making Same, Patent WO2009152217 A1, 2010.
[44] N. Perkas, M. Shuster, G. Amirian, Y. Koltypin, A. Gedanken, Sonochemical immobilization of silver nanoparticles on porous polypropylene, J. Polym. Sci. 46 (2007) 1719–1729.
[45] EPA, Secondary Drinking Water Regulations: Guidance for Nuisance Chemicals, U.S. Environmenal Protection Agency, 2013, http://water.epa.gov/drink/contaminants/secondarystandards.cfm.
[46] J. Schwinge, D.E. Wiley, D.F. Fletcher, Simulation of the flow around spacer filaments between narrow channel walls. 1. Hydrodynamics, Ind. Eng. Chem. Res. 41 (2002) 2977–2987.
[47] J. Schwinge, D.E. Wiley, D.F. Fletcher, Simulation of the flow around spacer filaments between channel walls. 2. Mass-transfer enhancement, Ind. Eng. Chem. Res. 41 (2002) 4879–4888.
[48] K.S. Suslick, The chemical effects of ultrasound, Sci. Am. 2 (1989) 80–86.
[49] C.N. Lok, C.M. Ho, R. Chen, Q.Y. He, W.Y. Yu, H. Sun, P.K.H. Tam, J.F. Chiu, C.M. Che, Silver nanoparticles: partial oxidation and antibacterial activities, J. Biol. Inorg. Chem. 12 (2007) 527–534.
[50] Total Organic Carbon measurements in seawater by Wet-chemical oxidation using the HiPerTOC, Application Note: 42110, 2007.
[51] X.X. Li, H. Nikaido, K. Williams, Silver-resistant mutants of *Escherichia coli* display active efflux of Ag+ and are deficient in porins, J. Bacteriol. 179 (1997) 6127–6132.
[52] A.T. Hendry, I.O. Stewart, Silver-resistant Enterobacteriaceae from hospital patients, Can. J. Microbiol. 25 (1979) 915–921.
[53] H.C. Flemming, Biofouling in water systems-cases, causes and countermeasures, Appl. Microbiol. Biotechnol. 59 (2002) 629–640.